# Microstructure and surface scaling in ballistic deposition at oblique incidence

Joachim Krug
*Theoretische Physik, Universität München, Theresienstrasse 37, 8000 München 2, Federal Republic of Germany*

Paul Meakin
*Central Research and Development Department, E.I. du Pont de Nemours and Company, Wilmington, Delaware 19880-0356*
(Received 21 February 1989)

Scaling properties of two-dimensional ballistic deposits grown at near-grazing angles of incidence are investigated analytically and numerically. We map the problem onto a system of coalescing Brownian particles and derive exact values for the static and dynamic surface exponents, $\zeta=1$ and $z=2$, and for the exponents characterizing the self-affine columnar microstructure, $\tau=\frac{4}{3}$, $\nu_{\parallel}=\frac{2}{3}$, and $\nu_{\perp}=\frac{1}{3}$. This implies that the average column width increases as the square root of the deposit thickness. The distribution of surface step heights and the angular variation of the deposit density are also obtained analytically. The predictions are confirmed by large-scale computer simulations. Qualitative arguments are given to explain the slow crossover behavior at intermediate angles of incidence, which leads to apparently continuously varying scaling exponents. The substructure exponents for deposits grown at normal incidence are derived from a general scaling relation. We find $\tau=\frac{7}{5}$, $\nu_{\parallel}=\frac{3}{5}$, and $\nu_{\perp}=\frac{2}{5}$, in agreement with previous numerical work.

## I. INTRODUCTION

It has been known for a long time[1] that the roughness and porosity of vapor-deposited thin films increase if the deposition process is carried out at oblique incidence. The deposit develops a characteristic microstructure[2] consisting of columnar grains. While its details clearly depend on material properties and deposition parameters, the microstructure is commonly believed[2] to result from the combined effects of self-shadowing[1] and limited atomic mobility. Thus it might be possible to capture some essential structural features in oversimplified theoretical models, such as the ballistic deposition model first introduced by Vold[3] in a different context. In this model, particles are added one by one to the deposit along randomly chosen, linear trajectories which form a fixed angle $\theta$ with the substrate normal. At the point of first contact with the deposit, the particles stick irreversibly. This corresponds to the limit of zero atomic mobility, or a very low substrate temperature.

Early computer simulations of such models[4,5] focused on the geometrical structure of the deposit. In particular, the dependence of the angle $\phi$, formed by the columnar grains with the substrate normal, on the angle of incidence $\theta$ was investigated. On the basis of their measurements of vapor-deposited aluminum films, Nieuwenhuizen and Haanstra[6] proposed the empirical relationship $\tan(\theta)=2\tan(\phi)$ (the "tangent rule"). This appeared to be confirmed by a number of experimental[2] and numerical[5] studies. However, other experiments[7-9] were in conflict with the tangent rule, indicating, in particular, that $\phi$ is not uniquely determined by $\theta$, but depends on, e.g., the substrate temperature as well.[7,8] In view of this, it is not too surprising that recent large-scale computer simulations[10,11] of the simplest ballistic deposition model have shown that no universal relation between $\phi$ and $\theta$ exists.

The more recent interest in simple computer models of irreversible aggregation and deposition was triggered by the observation of Witten and Sander[12] that statistically self-similar ("fractal"[13]) structures can be generated by such models. Although the internal structure of a ballistic deposit grown at normal incidence is uniform on all but quite short length scales,[14-16] its surface is statistically self-affine[13] and can be characterized by universal scaling exponents.[17,18] Moreover, the growth process itself decomposes the deposit into clusters which have a power-law mass and size distribution.[19] At oblique angles of incidence, these clusters separate and constitute the columnar morphology of the deposit.[11]

One of us (P.M.) recently presented the results of a simulation study[11] (henceforth referred to as I) of ballistic deposition at oblique incidence. The relationship between the angles $\phi$ and $\theta$ and the scaling properties of both the surface and the deposit substructure were investigated. One of the main observations was that the scaling exponents appear to change continuously with the angle of incidence and approach certain limiting values at near-grazing incidence, $\theta\rightarrow 90°$. The main objective of the present work is to present a simple theoretical picture of ballistic deposition at near-grazing incidence that allows us to determine exactly the scaling exponents (Sec. III A), the distribution of surface step heights (Sec. III B), and the angular variation of the deposit density (Sec. III C). The latter relates to the shape of clusters grown by ballistic deposition onto a point seed (Appendix).

In order to verify the theoretical predictions, we have carried out a series of simulations on finite strips and numerical measurements of the step-height distribution. Both lattice and off-lattice models for ballistic deposition onto an inclined substrate have been described previously in I. Most of the simulations were carried out using a two-dimensional (square) lattice model in which columns of the lattice are selected randomly and the site at a

 

height $h_i'$ given by

$$h_i' = \max(h_{i-1}, h_i + 1, h_{i+1}) \tag{1.1}$$

is filled to represent deposition in the $i$th column. Here, $h_i$ is the maximum $y$ coordinate for any of the occupied sites in the $i$th column. At the start of each simulation the site in the $i$th column given by

$$h_i = [i \tan(\theta)] \tag{1.2}$$

is occupied. Here, $\theta$ is the angle of incidence (angle of inclination of the substrate) and $[x]$ is the integer closest to $x$. In all our simulations, periodic boundary conditions were used in the lateral direction.

The information gained from these simulations is particularly valuable at intermediate angles of incidence, where the behavior is complex and only qualitative theoretical arguments can be given (Sec. IV). In Sec. II we introduce the surface and substructure scaling exponents and derive various exponent identities.[20] The treatment given is general and not restricted to ballistic deposition. In particular, we show that the substructure exponents $\nu_\parallel$ and $\nu_\perp$ are related to the dynamic surface exponent $z$ through $z = \nu_\parallel / \nu_\perp$, which is used to account for recent numerical results[19] at normal incidence. Some conclusions and open questions are presented in Sec. V.

Most of our results are restricted to deposition onto a line, i.e., $d = 2$ spatial dimensions. Numerically, this allows us to determine scaling exponents and other statistical properties with rather high accuracy. Theoretically, the main simplifying feature exploited in Sec. III is a mapping of the deposition process onto a system of interacting particles on the line. Such an approach, which is naturally limited to $d = 2$, has already proved to be useful in the analysis of other growth models.[10,21,22]

A number of continuum theories[2,23–25] have been proposed to account for the columnar morphology of vapor-deposited films. However, a linear-stability analysis[2] shows that column formation is driven by a short-wavelength instability, indicating the importance of the finite size of the deposited particles. The instability can be controlled by introducing some amount of surface diffusion.[24,25] The width of the columns is then determined by the diffusion length.[2,24,25] In the absence of such a length scale, the microstructure is scale invariant, with an average column width increasing as a power of the deposit thickness. As we will argue below, such a structure cannot, in principle, be captured in a continuum description.

## II. SCALING PROPERTIES OF THE GROWING SURFACE AND THE DEPOSIT SUBSTRUCTURE

As first noted by Family and Vicsek,[17] a growing surface can be characterized by two scaling exponents, which describe, respectively, its static and dynamic scaling properties. Starting from a flat substrate at time $t = 0$, the surface develops a stationary (time-independent) roughness on a length scale $\xi_\parallel$ that grows with time as

$$\xi_\parallel \propto t^{1/z} . \tag{2.1}$$

This defines[26] the dynamic exponent $z$. The magnitude $\xi_\perp$ of the transverse surface fluctuations on the scale $\xi_\parallel$ is determined by the (static) wandering exponent[27] $\zeta$ through

$$\xi_\perp \propto \xi_\parallel^{\zeta} . \tag{2.2}$$

Much of the work on surface growth and deposition processes has been aimed at determining the exponents $\zeta$ and $z$, which are expected to be universal for large classes of models.[18,21,22] As an application of (2.1) and (2.2), we consider the width of the active zone for a ballistic deposit grown from a substrate of linear dimension $L$. The active zone is defined[28] as the set of unoccupied surface sites at which growth can occur. The scaling properties of the active zone are the same as those of the surface, and the two terms will be used synonymously in the following. The width $\xi$ is given by

$$\xi(L,h)^2 = (1/L) \sum_{i=1}^{L} (h_i - h)^2 \tag{2.3}$$

where $h_i$ is the height of the active-zone site above the substrate site $i$ and $h$ is the mean deposit thickness, which is proportional to the time $t$. The growth process becomes stationary when the correlation length $\xi_\parallel$ is of the order of the system size $L$, i.e., by (2.1) when $h \simeq L^z$. In the transient regime ($h \ll L^z$) the width increases as

$$\xi \propto \xi_\parallel^{\zeta} \propto h^{\beta} , \tag{2.4}$$

with $\beta = \zeta / z$. In the stationary limit $h \gg L^z$ it saturates at a value

$$\xi_\infty \propto L^{\zeta} . \tag{2.5}$$

This is summarized in the scaling form[17,29]

$$\xi(L,h) = L^{\zeta} f(h / L^z) \tag{2.6}$$

where $f(x \to \infty) = \text{const}$ and $f(x \to 0) \propto x^{\beta}$.

A large class of interfacial growth processes can be described by the continuum equation of Kardar, Parisi, and Zhang.[18] In these cases the surface exponents are related by[10,20]

$$\zeta + z = 2 . \tag{2.7}$$

In the following we give an intuitive derivation of (2.7). For simplicity, we restrict our discussion to a one-dimensional surface, although the argument [and the relation (2.7)] is valid in arbitrary dimensions. On a macroscopic scale, a growth process is characterized by[22] the growth velocity $v = \partial h / \partial t$ as a function $v(u)$ of the surface slope $u = \partial h / \partial x$. Here, $h(x,t)$ measures the height of the surface above some (fixed) reference plane. Both $h(x,t)$ and $u(x,t)$ are averaged over some hydrodynamic volume that is large compared to the size of the particles. It follows that $u(x,t)$ satisfies a macroscopic conservation equation[22,30]

$$\frac{\partial}{\partial t} u(x,t) = \frac{\partial}{\partial x} v(u) = v'(u) \frac{\partial}{\partial x} u(x,t) . \tag{2.8}$$

A piece of the surface with slope $u$ translates along the $x$ axis with velocity $v'(u)$. We now consider a typical surface hump of height $\xi_\perp$ and width $\xi_\parallel$. The sides of the hump have slopes $u_0 \pm \xi_\perp/\xi_\parallel$, where $u_0$ is the average inclination of the surface. Their relative velocity is therefore

$$v'(u_0+\xi_\perp/\xi_\parallel)-v'(u_0-\xi_\perp/\xi_\parallel)\simeq v''(u_0)(\xi_\perp/\xi_\parallel) \tag{2.9}$$

since $\xi_\perp/\xi_\parallel \ll 1$. Thus the hump widens at a rate proportional to (2.9),

$$\dot{\xi}_\parallel \simeq \lambda(\xi_\perp/\xi_\parallel) , \tag{2.10}$$

with

$$\lambda = |v''(u_0)| . \tag{2.11}$$

As an example, consider a horizontal surface ($u_0=0$) that grows at a fixed speed $v_0$ in the direction of the local surface normal. Then $v=v_0\cos(\theta)$ with $\tan(\theta)=u$, and $\lambda=|v''(0)|=v_0$. The scaling relation (2.7) now follows by comparing (2.10) to (2.1) and (2.2). Physically, (2.7) demonstrates that if the surface is rough ($\zeta>0$), then its fluctuations spread *faster*[30] than diffusively ($z<2$). In exceptional cases it may happen[22] that $\lambda=0$. Then the coupling between static and dynamic fluctuations, as described by (2.10), does not take place and (2.7) is violated. In Sec. IV this will be shown to occur for ballistic deposition at near-grazing incidence.

A different kind of scaling description applies to the deposit substructure.[19] Suppose that at the beginning of the growth process the substrate sites are labeled by, e.g., their coordinates. Each newly added particle is then given the same label as the deposit particle to which it sticks. (If this prescription is not unique, one of the possible candidates is chosen according to some probabilistic or deterministic rule.) The deposit is thus subdivided into treelike clusters of particles that share the same label. The cluster-size distribution $n(s)$, giving the number of clusters of mass $s$, turns out to have a power-law decay

$$n(s) \propto s^{-\tau} , \tag{2.12}$$

where, typically,[31,32] $1<\tau<2$. Moreover, the average width $w$ and height $h$ of a cluster scale with its mass as

$$w(s) \propto s^{\nu_\perp}, \quad h(s) \propto s^{\nu_\parallel} . \tag{2.13}$$

We note that similar exponents occur in static models such as directed percolation and directed lattice animals.[33]

In the cases of interest here, both the individual clusters and the deposit as a whole are compact, with the fractal dimension equal to the spatial dimension $d$. As a consequence, the substructure exponents satisfy the scaling relations[19]

$$\nu_\parallel + (d-1)\nu_\perp = 1 \tag{2.14}$$

and

$$\tau = 2-\nu_\parallel , \tag{2.15}$$

leaving only one independent exponent. A third scaling law relating $\nu_\parallel$ and $\nu_\perp$ to the dynamic surface exponent $z$ can be obtained as follows. Consider a cluster which extends from the substrate to the surface of the deposit. The height $h$ of the cluster is then proportional to the time $t$ (or the deposit thickness) and its width $w$ may be identified with the surface correlation length $\xi_\parallel$. Comparing (2.1) with (2.13), we conclude that

$$\nu_\parallel/\nu_\perp = z . \tag{2.16}$$

Physically, this reflects the fact that the deposit substructure consists of "frozen" surface fluctuations. Thus (2.16) provides a quantitative example of how the properties of the active zone determine the bulk structure of a random aggregate.[28] A relation analogous to (2.16) links the directed animal exponents to the dynamic exponent of a one-dimensional lattice gas with negative fugacity.[34]

To conclude this section, we relate (2.16) to the numerical estimates for the substructure exponents obtained in Ref. 19 for ballistic deposition at normal incidence and Eden growth. For a one-dimensional surface ($d=2$) it is known that $z=\frac{3}{2}$ exactly in these models.[18,30,35] It follows then from (2.14)–(2.16) that

$$\nu_\perp = \tfrac{2}{5}, \quad \nu_\parallel = \tfrac{3}{5}, \quad \tau = \tfrac{7}{5} , \tag{2.17}$$

in excellent agreement with the numerical values,[19] $\nu_\perp=0.405$, $\nu_\parallel=0.610$, and $\tau=1.401$ for on-lattice ballistic deposition. In $d=3$, various numerical simulations[10,36–38] and a recent theoretical treatment[39] suggest that $z=\frac{5}{3}$. Using this value, we get

$$\nu_\perp = \tfrac{3}{11} \simeq 0.273, \quad \nu_\parallel = \tfrac{5}{11} \simeq 0.455, \quad \tau = \tfrac{17}{11} \simeq 1.545 , \tag{2.18}$$

very close to the results of Ref. 19 ($\nu_\perp=0.283$, $\nu_\parallel=0.452$, $\tau=1.566$). We shall see below that the scaling relations (2.14)–(2.16) continue to hold for ballistic deposition at oblique incidence, although the exponents differ from (2.17).

## III. DEPOSITION AT NEAR-GRAZING ANGLES OF INCIDENCE

As the angle of incidence of the particle trajectories with respect to the surface normal, $\theta$, varies from 0° to 90°, the deposit undergoes a striking transition from homogeneous to columnar morphology. The treelike clusters which form the deposit substructure become well separated and appear to grow independently of each other. The remarkable stability of the structure is illustrated in Fig. 1. Since the separation between clusters is much larger than their width, different clusters never collide. Moreover, there is hardly any tip splitting. If two branches form at the tip of a cluster, one of them is soon screened by the other and stops growing. The clusters grow at a fixed angle $\psi$ with respect to the particle beam, which has a value of about 33° for on-lattice deposition.[11] The origin of such a limiting angle will be discussed at the end of Sec. III A. First, we analyze an effective model of independently growing trees, which presupposes the existence of a structure like that shown in Fig. 1, and takes into account only the mutual long-range screening

between different clusters. The model is solvable by virtue of a mapping onto a system of coalescing Brownian particles on the line.

### A. Scaling of independently growing trees

We idealize the columnar structure as an array of rods growing at an angle $\phi=\theta-\psi$ with respect to the normal of the inclined substrate (Fig. 2). The substrate is taken to be infinitely extended. Since the sole interaction between rods is through mutual screening from the incoming flux, we need to follow only the motion of the tips. Once the tip of a rod is screened, the rod is frozen in its present state and grows no further. The tip of an "active" rod (which has not yet been screened) moves at some fixed average speed in the direction of growth. The fluctuations in the particle flux cause random-walk-like displacements from the average motion.

At a given instant of time, we label the active rods by an index $j$ and denote by $x_j(t)$ the $x$ coordinate of the tip of the $j$th rod. The $x$ axis is chosen perpendicular to the beam direction (Fig. 2). We interpret the $x_j(t)$ as the positions of particles on the real line. The particles have a drift to the left and a diffusion constant $D$. The drift is immaterial to the relative motion of the particles and may be eliminated by going to the moving frame. The mutual screening of neighboring rods has a simple image in the particle system: If the tip of the $j$th rod is screened by the $(j+1)$th, the corresponding particles coalesce and continue to move as one. We conclude that the tip positions $x_j(t)$ are a collection of *coalescing Brownian particles.*[40] A number of exact results[40–43] are known for this system, which carry over directly to the present context.

As can be seen from Fig. 2, the active zone consists of straight pieces with slope $-\text{cotan}(\psi)$ relative to the $x$ axis, interrupted by discontinuous jumps. Let us first focus on the straight segments. The projection of the $j$th segment onto the $x$ axis, $\Delta_j$, is equal to the distance between the corresponding Brownian particles,

$$\Delta_j=x_{j+1}-x_j \ . \tag{3.1}$$

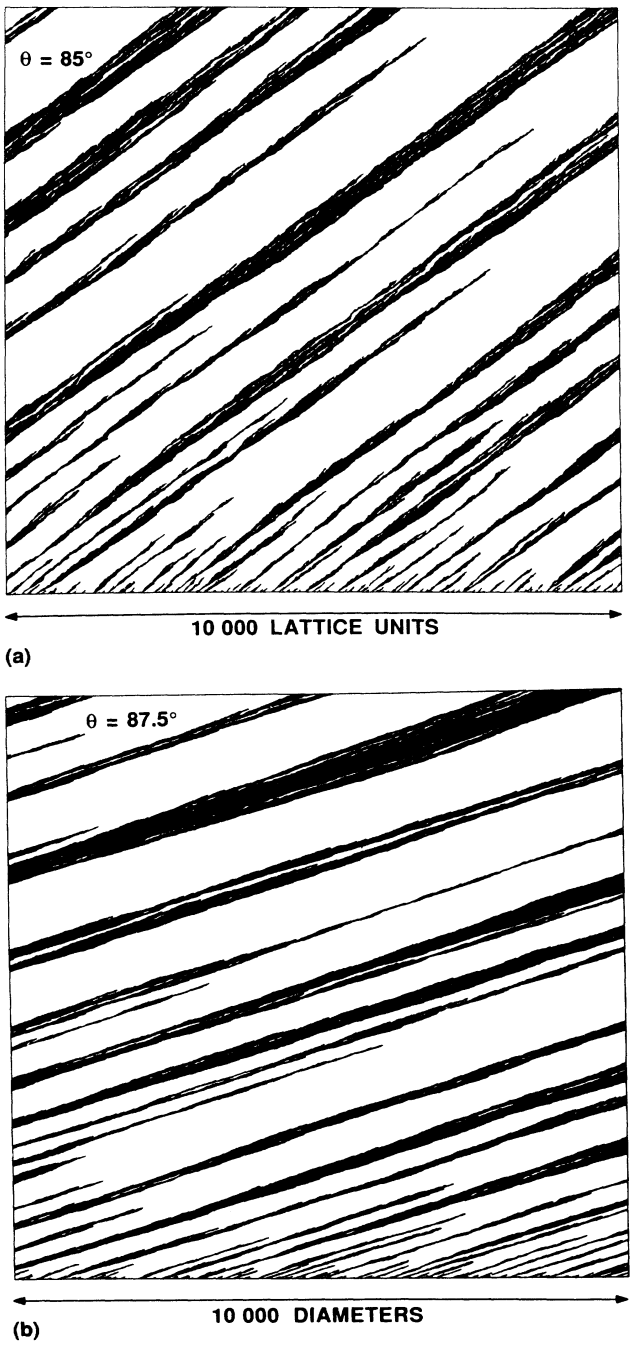


FIG. 1. Ballistic deposits grown on wide substrates at near-grazing angles of incidence. (a) Lattice model, $\theta=85°$. (b) Off-lattice model, $\theta=87.5°$.

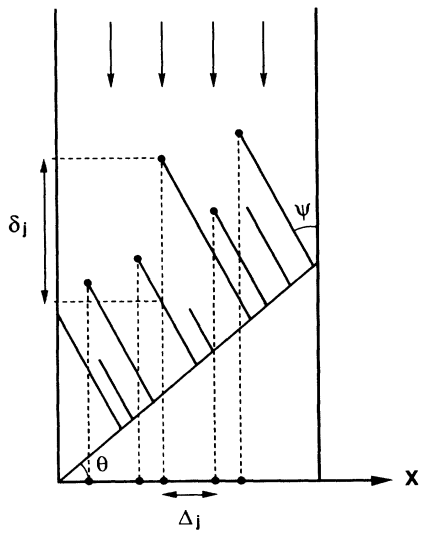


FIG. 2. Schematic view of a deposit of independently growing trees which interact only through screening. The mapping of the tip positions to a system of coalescing particles on the line is indicated.

In the long-time limit, the distribution function for the $\Delta_j$ is therefore[42]

$$P(\Delta,t)=(\pi/2)[\Delta/l(t)^2]\exp\{-(\pi/4)[\Delta/l(t)]^2\}\ , \tag{3.2}$$

where

$$l(t)=\sqrt{2\pi Dt} \tag{3.3}$$

is the average interparticle distance.[40] Clearly, $l$ corresponds to the correlation length $\xi_{\parallel}$ defined in (2.1). Thus we conclude that the dynamic surface exponent is

$$z=2\ , \tag{3.4}$$

i.e., surface fluctuations spread *diffusively*. The faster propagation of fluctuations that occurs at normal incidence, where $z=\frac{3}{2}$, is impeded by the columnar morphology.

The substructure exponents now follow from the scaling relations (2.14)–(2.16). We find

$$\nu_{\perp}=\tfrac{1}{3},\quad \nu_{\parallel}=\tfrac{2}{3},\quad \tau=\tfrac{4}{3}\ . \tag{3.5}$$

This implies, in particular, that the average width of the trees grows as the square root of the deposit thickness. Numerical estimates for $\nu_{\parallel}$ and $\tau$ were reported in I. The values are close to the predictions (3.5) for angles of incidence exceeding $\theta\simeq 75°$, e.g., $\nu_{\parallel}=0.699$ and $\tau=1.332$ at $\theta=80°$. We note that the same substructure exponents have been derived for the river-network model,[44] using a similar mapping to a system of Brownian particles.

Next, we turn our attention to the discontinuities in the active zone. Let $\delta_j$ denote the vertical jump from the tip of the $j$th active rod (Fig. 2). $\delta_j$ remains unchanged as the tip position $x_j(t)$ diffuses along the $x$ axis. Upon coalescence of $x_j$ and $x_{j-1}$, the jump which belongs to the surviving rod (the $j$th) is the sum $\delta_{j-1}+\delta_j$. Thus $\delta_j$ is an *additive* property of the Brownian particle $x_j$, which we may identify with the particle *mass*. Initially all particles have equal mass. In the course of the coagulation process, the masses of coalescing particles are added and a characteristic mass distribution[45] builds up. This will be discussed in the next section. The total mass is a constant of motion. It can be determined by noting that the average slope of the active zone is $\tan(\theta)$. Thus we have, for a strip of (horizontal) width $L$,

$$\sum_j[\delta_j-\mathrm{cotan}(\psi)\Delta_j]=L\tan(\theta) \tag{3.6}$$

which implies, using $\sum_j\Delta_j=L$,

$$\sum_j\delta_j=L[\mathrm{cotan}(\psi)+\tan(\theta)]\ . \tag{3.7}$$

Moreover, it follows from (3.6) that the average mass $\delta(t)=\langle\delta_j(t)\rangle$ is

$$\delta(t)=[\mathrm{cotan}(\psi)+\tan(\theta)]l(t)\propto t^{1/2}\ . \tag{3.8}$$

Since $\delta$ is the magnitude of a typical transverse surface fluctuation on the scale $l$, the relation (3.8) determines the wandering exponent $\zeta$ through $\delta\propto l^{\zeta}$ [cf. (2.2)]. Thus

$$\zeta=1\ , \tag{3.9}$$

and the short-time exponent $\beta=\zeta/z$ [cf. (2.4)] is

$$\beta=\tfrac{1}{2}\ . \tag{3.10}$$

As the surviving clusters have independent height fluctuations, the exponent is the same as for the random-deposition model.[17] However, in that model the surface is spatially uncorrelated, and the exponents $\zeta$ and $z$ are not defined. Values of $\beta$ close to $\frac{1}{2}$ were obtained both from the lattice simulations in I ($\beta=0.488$ at $\theta=87.5°$) and from off-lattice simulations[46] ($\beta=0.447$ without restructuring, $\beta=0.46$ with restructuring, at $\theta=85°$).

The wandering exponent $\zeta$ can also be estimated directly from (2.5) by measuring the stationary surface width $\xi_{\infty}$ as a function of the substrate size $L$. Simulations were carried out using strips of width $L=32$, 64, 128, 256, 512, and 1024 lattice units, and $\xi$ was measured in the stationary ($h\gg L^z$) limit. For the larger values of $L$, the fluctuations in $\xi$ are quite large, and quite large-scale simulations are required to reduce the statistical uncertainties to reasonably low levels. For $\theta=80°$ and $L=1024$, the width $\xi$ was obtained from four simulations in which a total of $1.4\times10^{10}$ sites were deposited. A similar set of simulations was carried out for angles of incidence of 87.5° and 70°. In addition, single large ($\simeq10^{10}$ sites) simulations were carried out for $\theta=85°$, $L=1024$ and $\theta=87.5°$, $L=2048$. The results are presented in Table I. A least-squares fit of the data for $\theta=87.5°$ gives $\zeta=0.98\pm0.03$. The behavior of $\zeta$ away from grazing incidence will be discussed below in Sec. IV.

We are now prepared to address the origin of the limiting growth angle $\psi$. Qualitatively, the direction of growth of a cluster is pushed towards the surface normal, i.e., $\psi>0$, due to partial screening of the particle flux by the cluster in front of it.[2] For a more quantitative treatment, we supplement the rods in Fig.2 by tips of finite extension, which we for simplicity idealize as circular discs of radius $R$. We pick a pair of adjacent active rods and fix their horizontal distance $\Delta$. If $\Delta<2R$, part of the first disk is screened by the second. The center of gravity of the mass deposited onto the disk then determines the momentary growth angle of the first rod as

$$\tilde{\psi}(\Delta)=\frac{1}{\Delta}\int_{R-\Delta}^{R}dx\ \arcsin(x/R) \tag{3.11}$$

where we have used that the $x$ coordinates of the particle

TABLE I. Steady-state surface width $\xi_{\infty}$ as a function of the horizontal strip width $L$ for various angles of incidence $\theta$. The substrate length is $L/\cos(\theta)$ in each case.

| $L$ | $\theta=70°$ | $\theta=80°$ | $\theta=87.5°$ |
|---|---|---|---|
| 32 | 15.47 | 40.19 | |
| 64 | 26.8 | 76.09 | 388.3 |
| 128 | 45.08 | 142.45 | 772.5 |
| 256 | 73.4 | 264.3 | 1553.0 |
| 512 | 118.4 | 486.5 | 2980 |
| 1024 | 180.4 | 873.4 | 5892 |

trajectories are uniformly distributed on the line. The average growth angle of the structure is now obtained by averaging (3.11) relative to the distribution (3.2),

$$\psi = \int_0^{2R} d\Delta\, \tilde{\psi}(\Delta) P(\Delta,t)\ , \tag{3.12}$$

which depends only on the ratio $R/l$. The limiting behavior of (3.12) is $\psi \to 0$ for $R \ll l$ and $\psi \to \pi/2$ for $R \gg l$. We conclude that a nontrivial growth angle ($0 < \psi < \pi/2$) emerges only if the width of the clusters, $R$, scales as their mutual distance $l$. In the present case both $R$ and $l$ grow as $t^{1/2}$ [Eqs. (3.3) and (3.5)], so the limit $r = \lim_{t\to\infty} R/l$ exists and is nonzero. We note that the whole argument does not depend on the angle of incidence, showing that $\psi$ becomes independent of $\theta$ in the regime where the clusters are well separated.[11] This is confirmed by the exact solutions for deposition onto narrow strips presented below in Sec. III C. On the other hand, $r$ clearly does depend on model details, so $\psi$ is not universal.[11] Setting $r = 1$ in (3.12) yields $\psi = 34°$, fortuitously close to the numerical value for the lattice model.

We note that the surface exponents (3.4) and (3.9) do *not* satisfy the scaling relation (2.7). This is clearly due to the strongly discontinuous structure of the active zone, which does not permit a continuum description. Stated differently, for deposition at near-grazing incidence the active zone is dominated by short-wavelength rather than by long-wavelength fluctuations.[2] This has important implications for the distribution of surface step heights, which we outline in the following.

### B. Step-size distribution

In this section we study the distribution of step heights

$$\sigma_i = |h_i - h_{i+1}| \tag{3.13}$$

for the lattice model of ballistic deposition. Here, $h_i$ is the height of the active-zone site in the $i$th lattice column, measured from the horizontal $x$ axis along the column (in the direction of the incoming particle trajectories). At normal incidence ($\theta = 0$) the $\sigma_i$ are exponentially distributed, with an average step size of order unity.[10] Starting from a flat substrate, the distribution becomes stationary after a relaxation time that is independent of the system size. The step-size distribution has no influence on the long-wavelength fluctuations of the surface, which dominate the long-time behavior of the surface width. Thus the scaling exponents $\zeta$ and $z$ are the same both for standard ballistic deposition and a related model[10] where the step heights are constrained to $\sigma_i = 1$. In fact, the irrelevance of short-range details is decisive for the applicability of continuum theories.[18]

The situation is clearly quite different at near-grazing incidence, where the deposit consists of separated clusters. There are now two different kinds of steps $\sigma_i$, depending on whether the two active-zone sites belong to the same cluster or not. In the former case, $\sigma_i$ is again of order unity. If, however, $h_i$ and $h_{i+1}$ belong to different clusters, then the active zone has a discontinuity at site $i$, with an average magnitude growing as $t^{1/2}$ [cf. (3.8)]. Thus we expect the step-size distribution to consist of two parts: one corresponding to the small steps, which becomes stationary as $t \to \infty$, and one corresponding to the discontinuities in the active zone, which has a mean proportional to $t^{1/2}$ and never becomes stationary.

This is illustrated in Fig. 3(a), where step-size distribu-

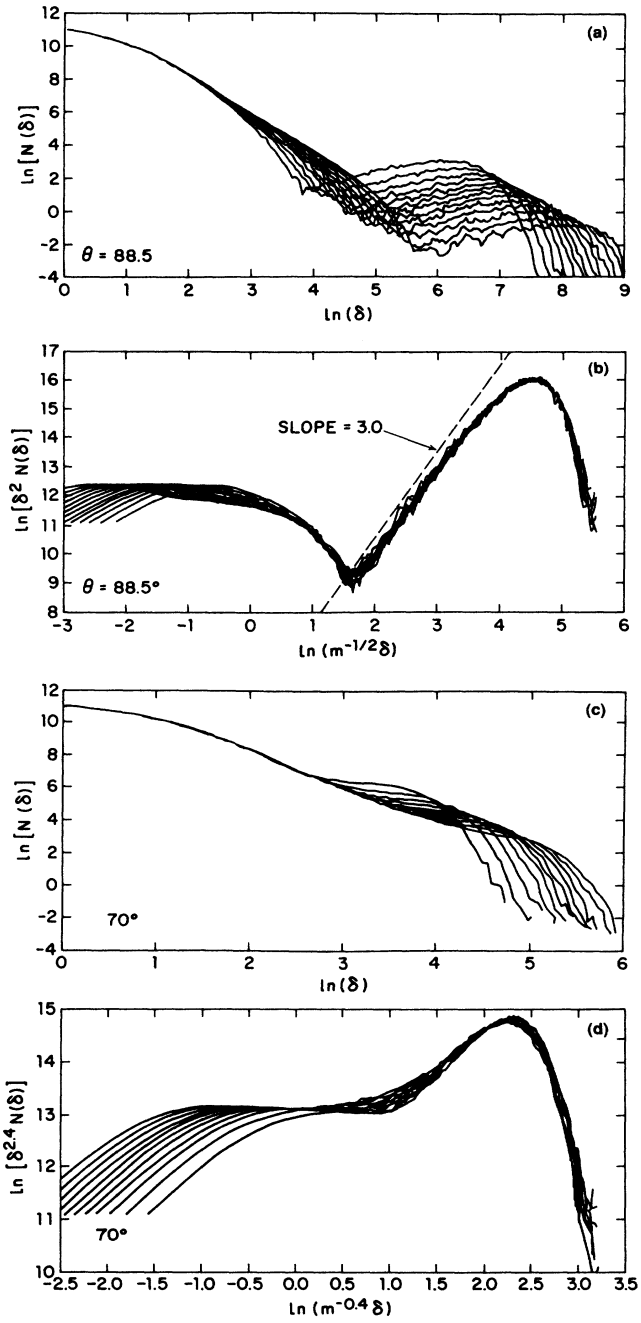


FIG. 3. Numerical results for the distribution of surface step heights. The lattice width was $L = 2^{18} = 262\,144$ in all cases. (a) Step-size distributions measured at different times for $\theta = 88.5°$. (b) The data of (a) scaled according to (3.14). (c) Step-size distributions measured at different times for $\theta = 70°$. (d) The data of (c) scaled according to (4.6).

tions measured at different times are superimposed. Simulations were carried out on wide strips ($L=2^{18}$ or 262 144 sites) for angles of incidence of 30°, 45°, 60°, 70°, 80°, 85°, 87.5°, and 88.5°. In these simulations $10^9-2\times10^9$ sites were deposited for each value of $\theta$. The step-size distribution was measured each time $t$ exceeded an integer (each time the total number of deposited sites exceeded an integer multiple of $L$) and was averaged over 2.5% increments in the total mass (number of deposited sites).

Here we focus on the large steps. Let $N(\delta,t)$ denote the number of large steps of height $\delta$ at time $t$. Since the average step height grows as $t^{1/2}$, we write this in the scaling form

$$N(\delta,t)/L=\delta^{-2}f(\delta/t^{1/2}) , \tag{3.14}$$

where $L$ is the (horizontal) lattice size and the exponent $-2$ of the prefactor arises from the normalization condition (3.7). The scaling function $f$ can be determined from the analogy with coalescing Brownian particles. As explained in the preceding section, the problem is then reduced to finding the mass distribution of the particle system. This was recently achieved by Spouge.[43] Here we use his result for coalescing Brownian particles on a one-dimensional lattice that is completely occupied by particles of unit mass at $t=0$. The concentration of particles of mass $k$ at time $t$ is given by[43]

$$c_k(t)=\exp(-4Dt)[I_{k-1}(4Dt)-I_{k+1}(4Dt)] , \tag{3.15}$$

where $I_k$ is a modified Bessel function of order $k$ and $D$ is the diffusion constant. Using the asymptotics of $I_k(x)$ for large $x$ and the recursion relation[47]

$$I_{k-1}(x)-I_{k+1}(x)=(2k/x)I_k(x) , \tag{3.16}$$

it can be shown that in the scaling limit $t\to\infty$, $k\to\infty$, $k^2/t\to$const, (3.15) reduces to

$$c_k(t)\simeq(4\pi)^{-1/2}[k/(2Dt)^{3/2}]\exp(-k^2/8Dt) . \tag{3.17}$$

This may also be derived using the duality to the voter model.[41] Comparing (3.17) to (3.14) and using (3.7) and (3.8), it follows that the scaling function is

$$f(x)=C^{-2}(32\pi D^3)^{-1/2}x^3\exp[-x^2/(8DC^2)] \tag{3.18}$$

with $C=\text{cotan}(\psi)+\tan(\theta)$. In Fig. 3(b) we show a scaling plot of $\delta^2N(\delta,t)$ as a function of $\delta/t^{1/2}$. The small-$x$ behavior $f(x)\propto x^3$ is clearly seen, as well as the Gaussian maximum of the scaling function. From the position of the maximum the tip diffusion constant $D$ can be estimated. We find $D=0.43$ for $\theta=88.5°$, $D=0.41$ for $\theta=87.5°$, and $D=0.35$ for $\theta=85°$. As $\theta$ decreases away from grazing incidence, the large step part of the distribution becomes less pronounced and eventually vanishes. This will be addressed in Sec. IV.

### C. Steady-state structure and deposit density

If deposition is carried out on a strip of horizontal width $L$, the growth becomes stationary after a relaxation time of the order $L^z$ (cf. Sec. II). At near-grazing incidence, the competitive screening effects lead to a steady-state structure that consists of a single large cluster. The periodic (helical) boundary conditions force the cluster to wind around the strip, thus forming a periodic pattern of stripes and voids as shown in Fig. 4(a). In this section we give a quantitative characterization of the steady-state structure, based on analytical results for $L=1$ and 2.

It is useful to think of unwrapping the strip in Fig. 4(a) along the $x$ axis, thus producing a pattern of horizontal period $L$. From this point of view, deposition occurs simultaneously at every $L$th column of the infinitely extended lattice. This amounts to imposing a long-wavelength cutoff on the fluctuations of the particle flux. We see that the finite system size acts as a noise-reduction mechanism that selectively suppresses the *long-wavelength* components of the noise. This is in contrast to the noise-reduction method introduced by Wolf and Kertész[36,48] and applied in I to ballistic deposition, which is intended to suppress (irrelevant) *short-wavelength* fluctuations. The two mechanisms coincide, however, in the limit of infinite noise reduction, $L=1$ and $m=\infty$, respectively, where $m$ is the noise-reduction parameter.[48] Then the growth becomes deterministic.[21] We start from the inclined substrate, Eq. (1.2). For non-negative integer values of $n=\tan(\theta)$, all height variables $h_i$ have the same dynamics given by (1.1),

$$h(t+1)=\max(h(t)+1,h(t)+n) . \tag{3.19}$$

Thus the growth velocity is

$$v(\theta)=\begin{cases}1, & \theta\le45°\\ \tan(\theta), & \theta\ge45°\end{cases} \tag{3.20}$$

which is easily shown to hold for arbitrary $\theta$, $0\le\theta<90°$. Since time is counted as $t=M/L$, where $M$ is the number of deposited particles, the deposit density is

$$\rho(\theta)=1/v(\theta) . \tag{3.21}$$

For $\theta\le45°$ the growth proceeds layerwise and the deposit is maximally compact ($\rho=1$). For $\theta>45°$ the mutual screening of growth sites leads to a microstructure of needles growing perpendicular to the particle flux [Fig. 5(a)]. Thus at large angles of incidence the deposit consists of well-separated "clusters" that grow at a fixed angle

$$\psi_1=90° \tag{3.22}$$

with respect to the particle beam. The large value of $\psi_1$ is in qualitative agreement with the observation in I that strong noise reduction tends to increase the growth angle $\psi$.

The case $L=2$ is more interesting. Let $n=2\tan(\theta)$ be a non-negative integer. Then the two height variables $h_1,h_2$ evolve according to

$$\begin{aligned}h_1(t+1)&=\max(h_1(t)+1,h_2(t)) ,\\ h_2(t+1)&=\max(h_2(t)+1,h_1(t)+n) .\end{aligned} \tag{3.23}$$

At each time step, one of the two columns (or one of the two sublattices, if we think of the equivalent process on the infinite lattice) is chosen at random and updated fol-

lowing (3.23). The dynamics is most easily described in terms of the step variable

$$\sigma(t)=h_2(t)-h_1(t)\ , \tag{3.24}$$

which performs a random-walk-like motion on the integers. There are no transitions into the region $0<\sigma<n$. Thus, in the steady state, $\sigma\leq 0$ or $\sigma\geq n$. Qualitatively, the step-size distribution is therefore similar to that discussed in the preceding section, with a small step ($\sigma\leq 0$) and a large step ($\sigma\geq n$) part. We introduce the probabilities

$$p_k=\text{Prob}(\sigma=-k)=\text{Prob}(\sigma=n+k)\ , \tag{3.25}$$

$k=0,1,2\ldots$. These depend only on whether $n=0$ or $n\geq 1$. For $n=0$, the transition probabilities $\Gamma(k\rightarrow k')$ are given by

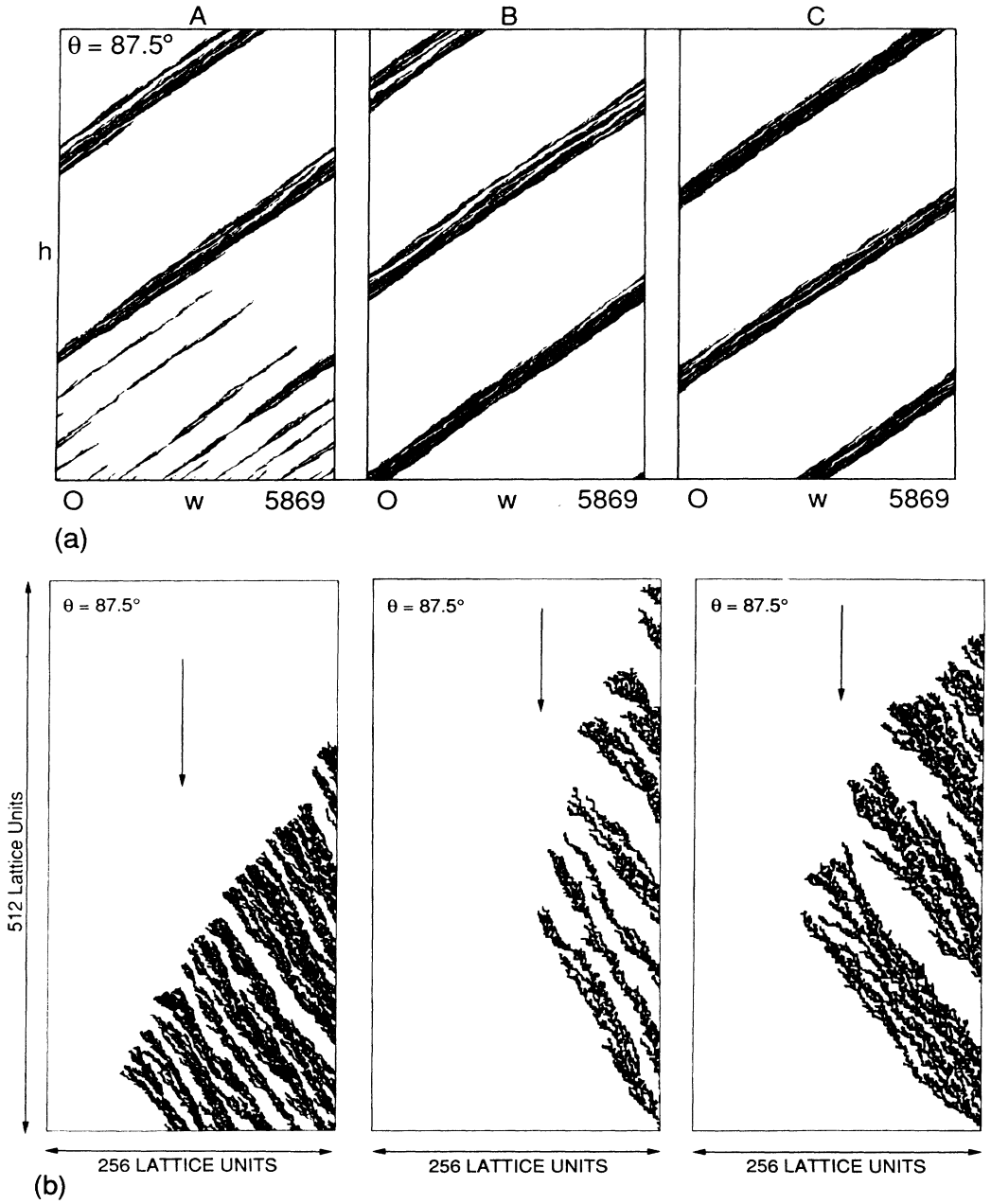


FIG. 4. Steady-state structure at $\theta=87.5°$. (a) Deposit grown on a strip of horizontal width $L=256$. The patterns are displayed in an orientation in which the substrate is horizontal. The substrate length is $L/\cos(\theta)=5869$. The height range is 0–10 000, 40 000–50 000 and 90 000–100 000 for parts *A*, *B*, and *C*, respectively. (b) Tip of steady-state clusters grown on strips of width $L=512$. The arrows indicate the direction of the incoming particle beam. Note that the orientation of the figure differs from (a).

$$\Gamma(0\rightarrow 1)=1 \tag{3.26a}$$

and

$$\Gamma(k\rightarrow k+1)=\Gamma(k\rightarrow 0)=\tfrac{1}{2} \tag{3.26b}$$

for $k\geq 1$. From (3.26a) it follows that $p_0=p_1$, and (3.26b) yields $p_{k+1}=p_k/2$ for $k\geq 1$. Thus the stationary distribution is

$$p_0=\tfrac{1}{3};\quad p_k=\tfrac{1}{3}2^{-(k-1)},\quad k\geq 1\ . \tag{3.27}$$

For $n\geq 1$, the transition rates are given by (3.26b) for all $k$ including $k=0$, and, consequently,

$$p_k=2^{-(k+1)} \tag{3.28}$$

for all $k\geq 0$.

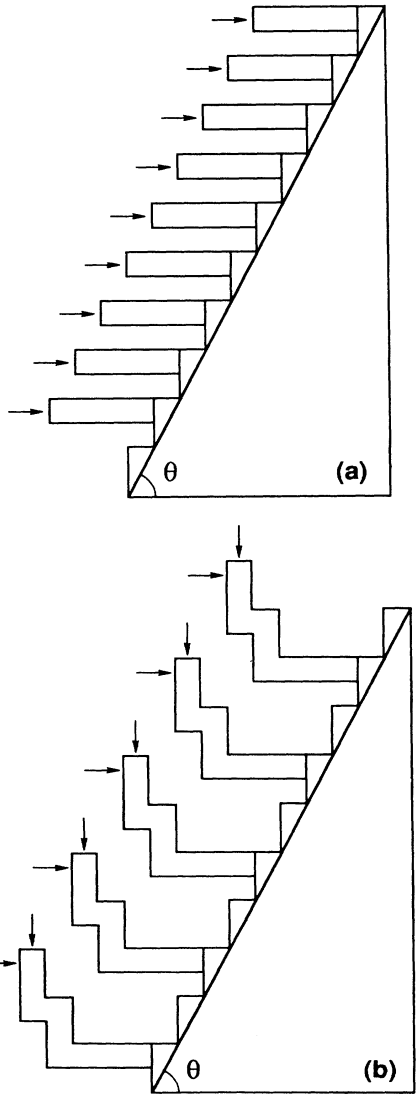


FIG. 5. Periodic structure generated by deposition on strips of width (a) $L=1$ and (b) $L=2$, with helical boundary conditions. The unscreened growth sites are indicated by arrows.

All quantities of interest in the $L=2$ model can be calculated from the $p_k$. In particular, the growth velocity is

$$v_n=1+n/2 \tag{3.29}$$

for $n\geq 1$, and

$$v_0=\tfrac{4}{3} \tag{3.30}$$

for $n=0$. The deposit is porous ($\rho<1$) at normal incidence also. At angles between $\theta=0$ and $\theta=\theta_0=\arctan\frac{1}{2}$ ($n=1$), the growth velocity interpolates linearly between $v_0$ and $v_1$. Thus we have, for $0\leq\theta<90°$,

$$v(\theta)=\begin{cases}[4+\tan(\theta)]/3, & \theta<\theta_0\\ 1+\tan(\theta), & \theta\geq\theta_0\ .\end{cases} \tag{3.31}$$

As for $L=1$ [Eq. (3.20)] there is a break in slope at $\theta_0=\arctan(1/L)$.

If $n\geq 2$, the forbidden region $0<\sigma<n$ in the steady-state distribution of $\sigma$ leads to the formation of voids. Suppose that at some time $h_1(t)\geq h_2(t)$. Then the next deposition event onto the second column yields, according to (3.23), $h_2=h_1+n$, and provided that $n\geq 2$ ($\theta\geq 45°$) a void is formed. The corresponding unwrapped periodic pattern is shown in Fig. 5(b). In contrast to the case $L=1$, where each needle could grow only at the side edge of the leftmost particle, the needles now have two unscreened growth sites, at the side edge and at the top edge of the tip, which are chosen with equal probability. Thus the microstructure is an array of parallel directed random walks, with an average orientation

$$\psi_2=45° \tag{3.32}$$

with respect to the beam direction. This is considerably closer than (3.22) to the asymptotic (large $L$) limiting angle $\psi\simeq 33°$.

We return now to the case of general (large) $L$ and discuss in some detail the emergence of the striped steady-state structure. As usual, the strip is oriented in the direction of the particle beam, with helical boundary conditions in the transverse direction. Consider the moment when the tip of a new stripe is just about to enter the strip at the right-hand boundary [Fig. 4(b)]. It moves across the strip at a transverse velocity $v_\perp$. For the lattice model, it is easy to see that $v_\perp=1$. The lower edge of the cluster forms an angle with the strip direction which we identify as the limiting angle $\psi$. The overall shape of the cluster is discussed in the Appendix. Eventually the cluster hits the left boundary and reenters the strip on the right. At this point the rightmost part of the cluster has received a total flux of $L/v_\perp$ particles per unit strip width. It is screened by the reentrant tip and grows no further. Thus the mass contained in a complete stripe is $L^2/v_\perp$. The volume occupied by the stripe and the corresponding void is $L^2[\mathrm{cotan}(\psi)+\tan(\theta)]$. This determines the density $\rho$ of the structure or, equivalently, the growth velocity $v=1/\rho$ as a function of $\theta$,

$$v(\theta)=v_\perp[\mathrm{cotan}(\psi)+\tan(\theta)]\ , \tag{3.33}$$

which is expected to hold for large enough $\theta$. Indeed, the

exact expressions (3.20) and (3.31) are of this form (with $v_\perp = 1$) in the regime $L\tan(\theta) > 1$. For $L = 1$, $\psi = \psi_1 = 90°$ and thus $v = \tan(\theta)$. For $L = 2$, $\psi = \psi_2 = 45°$ and $v = 1 + \tan(\theta)$. To test (3.33) for large $L$, we have grown large deposits ($10^8$ particles) on a strip of width $L = 1000$ with $0 \le \tan(\theta) \le 10$. Some of the results are shown in Fig. 6, together with the exact formulas (3.20) and (3.31). For $\tan(\theta) \ge 2$, the agreement with (3.33) is essentially perfect. A least-squares fit gives a value of 1.0007 for the prefactor of $\tan(\theta)$, and the constant term is $\cot(\psi) = 1.600 \pm 0.007$, corresponding to an angle $\psi = 32.0°$, in good agreement with previous estimates.[11] Similar results were obtained from a simulation of smaller deposits ($L = 1000$, $5 \times 10^6$ particles) in the range $0 \le \tan(\theta) \le 200$.

Conversely, (3.33) now provides us with a convenient method to determine the limiting angle $\psi$ from a measurement of the steady-state growth velocity. In Table II we give values for $\psi$ and the deposit density at normal incidence, $\rho_0$, as functions of the strip width $L$. Both $\psi$ and $\rho_0$ decrease with increasing $L$. We observe that the ratio $\tan(\psi)/\rho_0$ appears to be independent of $L$.

We have checked that (3.33) can be fitted to the data obtained in Ref. 46 for off-lattice deposition with and without restructuring, for large enough angles $\theta$. In these cases $v_\perp < 1$. A similar angular variation of the density has also been observed in vapor-deposition experiments.[7] We should mention that it is not obvious that (3.33), which was derived in the stationary limit $t \gg L^2$, also applies to deposition on an infinite (large) substrate with $t \ll L^2$. However, the same expression can be derived from the approximate model of Sec. III A (Fig. 2) by noting that $v_\perp$ is the drift velocity of the Brownian particles. Numerical simulations on wide strips also confirm (3.33),

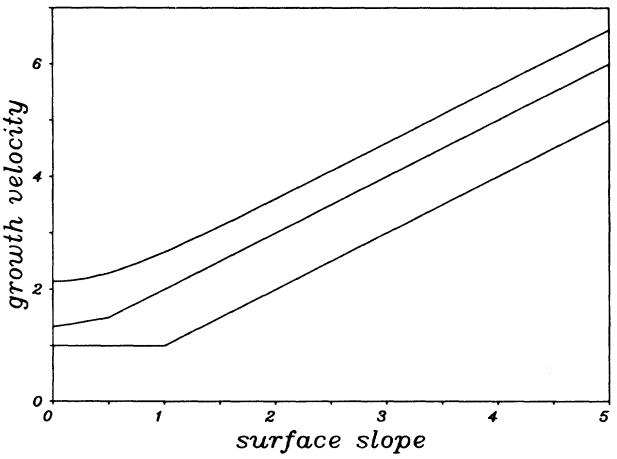


FIG. 6. Vertical growth velocity $v(\theta)$ as a function of the surface slope $\tan(\theta)$. From bottom to top the width of the strip is $L = 1$, 2, and 1000. The results for $L = 1$ and 2 are exact [Eqs. (3.20) and (3.31)]. For $L = 1000$, $\tan(\theta)$ was varied in steps of 0.1 in the range $0 \le \tan(\theta) \le 2$ and in steps of 1 in the range of $2 \le \tan(\theta) \le 5$. A deposit of $10^8$ particles was grown for each value of $\tan(\theta)$.

TABLE II. Limiting growth angle $\psi$ and deposit density at normal incidence, $\rho_0$, as functions of the strip width $L$. The results for $L = 1$ and 2 are exact. For the other values of $L$, a cluster of more than $10^5 L$ particles was grown for each integer value of $0 \le \tan(\theta) \le 50$ ($L = 3, 5$), respectively, $0 \le \tan(\theta) \le 12$ ($L = 5$–$100$). This gives the growth velocity $v(\theta)$. Then $\rho_0 = 1/v(0)$ and $\psi$ was determined by fitting $v(\theta)$ [for $\tan(\theta) \ge 2$] to (3.33). The fit was better than 1% in all cases.

| $L$ | $\psi$ (deg) | $\rho_0$ | $\tan(\psi)/\rho_0$ |
|---|---|---|---|
| 1 | 90 | 1 | |
| 2 | 45 | $\frac{3}{4}$ | $\frac{4}{3}$ |
| 3 | 40.9 | 0.661 | 1.31 |
| 5 | 37.9 | 0.584 | 1.33 |
| 10 | 34.4 | 0.527 | 1.30 |
| 20 | 33.4 | 0.497 | 1.33 |
| 50 | 32.4 | 0.482 | 1.32 |
| 100 | 32.1 | 0.475 | 1.32 |

indicating that the deposit density becomes stationary on a time scale independent of $L$, even if the steady-state structure has not yet been reached.

In the Appendix we show that $v(\theta)$ is related to the shape of the fanlike clusters which grow by ballistic deposition onto a point seed.[14,23] As an immediate consequence, we rederive Eq. (3.33) for large angles $\theta$ and estimate its range of validity. It is seen in Fig. 6 that deviations from the linear form (3.33) occur for $\tan(\theta) \le 2$. In this regime, collisions between substructure trees can no longer be neglected, and the scaling behavior changes. This is discussed in the next section.

## IV. CROSSOVER BEHAVIOR

At intermediate angles of incidence, the surface is subject to two conflicting mechanisms. As the density increases, the substructure trees tend to come into contact, allowing the surface fluctuations to spread more rapidly. The surface becomes smoother and the deposit more homogeneous. The corresponding length scale $\xi_\parallel^{(1)}$ follows from (2.10) with $\xi_\perp \propto \xi_\parallel^{1/2}$ for a continuous, one-dimensional surface,

$$\xi_\parallel^{(1)}(t) \propto (\lambda t)^{2/3} . \tag{4.1}$$

On the other hand, nonlocal screening still generates discontinuities in the active zone which impede the lateral spread of fluctuations. The length scale $\xi_\parallel^{(2)}$ associated with this process is the typical distance between two such discontinuities, from (3.3),

$$\xi_\parallel^{(2)}(t) \propto t^{1/2} . \tag{4.2}$$

Since (4.1) grows more rapidly with time than (4.2), one might expect the lateral spread of fluctuations to dominate the long-time behavior of the surface. The scaling exponents would then cross over to the values predicted by the continuum theory, $z = \frac{3}{2}$ and $\zeta = \frac{1}{2}$, on a time scale $t_c$ determined by $\xi_\parallel^{(1)}(t_c) \propto \xi_\parallel^{(2)}(t_c)$, i.e.,

$$t_c \propto \lambda^{-4} . \tag{4.3}$$

However, as noted above in Sec. II, the coupling constant $\lambda$ may actually vanish. In general, it is given by the second derivative of the growth velocity $v$ with respect to the surface slope $u$ [Eq. (2.11)]. In the present case, $u=\tan(\theta)$, and we know from (3.33) that $v(u)$ is a *linear* function of $u$ for large enough angles. It is difficult to extract the second derivative of $v(u)$ from noisy numerical data, but our simulation results (cf. Fig. 6) do indicate that $v''(u)$ is smaller than the statistical uncertainties for $\tan(\theta)\geq 2$. Thus in this range the crossover time $t_c$ is essentially infinite. Although the columnar morphology is, in principle, unstable with respect to the lateral spread of long-wavelength fluctuations, the crossover does not take place due to the smallness of the coupling. In that sense, the columnar morphology constitutes a *metastable* state of the system.

This picture is in qualitative agreement with the numerical results presented in I. There, an apparently continuous variation of the scaling exponents was found as a function of $\theta$. In particular, the measurement of the surface width $\xi\propto t^{\beta}$ as a function of time showed no sign of a crossover of $\beta$ towards the value at normal incidence, $\beta=\frac{1}{3}$, for $\theta\geq 60°$. The substructure exponents $\tau$ and $\nu_{\parallel}$ were also found to vary continuously from their values at normal incidence [Eq. (2.17)] to values close to (3.5) over the range $45°\leq\theta\leq 75°$. Since $\beta=\zeta/z$ and $z$ is related to the substructure exponents through (2.16), $\zeta$ can be calculated from the measured values of $\beta$ and $\tau$ according to

$$\zeta=\beta(2-\tau)/(\tau-1)\ . \tag{4.4}$$

For comparison, we have determined $\zeta$ directly from the steady-state width of the active zone (Table I). The results are summarized in Table III. It is seen that the measured values are fully consistent with the scaling relation, indicating that the scaling theory of Sec. II also applies to the situation at intermediate angles of incidence.

Some insight into the nature of the fluctuations which tend to destabilize the columnar morphology can be gained from the approach of the surface width to its steady-state value $\xi_{\infty}$. In Fig. 7 we show the time evolution of $\xi$ on a strip of width $L=1024$ for (a) $\theta=87.5°$ and (b) $\theta=80°$. In both cases there is an initial power-law increase, followed by an intermediate regime of very strong fluctuations. At this stage there is only a small number of growing clusters left in the system, and $\xi$ makes a jump every time a cluster is lost through screening. For $\theta=87.5°$ the system finally settles in the steady state, with a single cluster winding around the strip as described in Sec. III C. Correspondingly, the surface width saturates and stays constant. In contrast, for $\theta=80°$ the surface width continues to fluctuate by a factor 2 and more. We interpret these fluctuations as being due to occasional splitting of the single surviving cluster into two branches. This results in a sharp drop in $\xi$, followed by an increase when eventually one of the two branches is screened by the other. It is this "intermittent" behavior which effectively lowers the exponent $\zeta$. Due to the conflicting mechanisms described above, the system is unable to settle in a proper steady state with a well-defined value of $\zeta$.

The step-size distribution changes in two ways as $\theta$ is decreased away from grazing incidence. Firstly, the part of the distribution corresponding to the large steps, $N(\delta,t)$, becomes less pronounced. Secondly, the scaling form (3.14) for $N(\delta,t)$ has to be modified. As long as the large steps exist, they will dominate the long-time behavior of the surface width. Thus the average step height grows as

$$\langle\delta_j(t)\rangle\propto\xi(t)\propto t^{\beta}\ , \tag{4.5}$$

where the appropriate (effective) value of $\beta$ must be used for a given angle of incidence. Then (3.14) is generalized to

$$N(\delta,t)/L=\delta^{-\mu}f(\delta/t^{\beta})\ . \tag{4.6}$$

The exponent $\mu$ is determined through a normalization condition. The total number of large steps equals the number of clusters, which decays as $t^{-1/z}$ [cf. (2.12) and

TABLE III. Effective wandering exponent $\zeta$ for different angles of incidence $\theta$. The numbers in the first column, (1), were obtained from a fit of the data in Table I. Those in the second column, (2), were calculated from the values of $\beta$ and $\tau$ reported in I, using the scaling relation (4.4).

| $\theta$ (deg) | $\zeta^{(1)}$ | $\zeta^{(2)}$ |
|---|---|---|
| 87.5 | 0.98±0.03 | 1.04±0.05 |
| 80.0 | 0.89±0.01 | 0.89±0.04 |
| 70.0 | 0.71±0.03 | 0.72±0.03 |

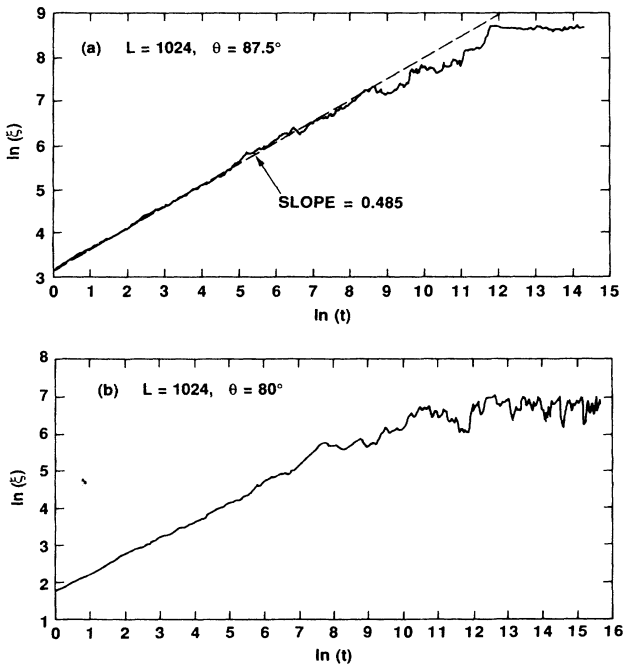


FIG. 7. Approach of the surface width $\xi$ to its equilibrium value $\xi_{\infty}$ on a strip of width $L=1024$. (a) $\theta=87.5°$ and (b) $\theta=80°$.

(2.13)]. This gives

$$\mu = 1 + 1/\zeta \ . \tag{4.7}$$

Thus $\mu > 2$ if $\zeta < 1$, indicating that the total mass in the related system of Brownian particles, i.e., the sum of (large) step heights (3.7), is no longer conserved. It decays as $t^{-(1-\zeta)/z}$ (cf. Ref. 21).

Figure 3(d) shows that the numerical data are well represented by (4.6) at least for $\theta \geq 70°$. At smaller angles, the large steps become increasingly difficult to detect.

## V. CONCLUSIONS

We have presented a detailed study of ballistic deposition at near-grazing angles of incidence. The columnar microstructure was found to be scale invariant, with the average column width increasing as the square root of the deposit thickness. This confirms an earlier conjecture[14] that ballistic aggregates, while having a finite density, may possess structure on all length scales. The surface and substructure scaling exponents were determined exactly, as well as structural properties of the deposit, such as the step-size distribution and the deposit density. All theoretical predictions compare favorably with the results of large-scale simulations.

The situation at intermediate angles of incidence appears to be more complex. The deposit can be consistently described by continuously varying exponents which satisfy the expected general scaling relations. We have attributed the peculiar marginal stability[2] of the columnar morphology to a competition between lateral growth and nonlocal screening. Further clarification of this point would certainly be welcome.

For obvious practical and theoretical reasons, it is of great interest to extend the present work to deposition onto two-dimensional substrates. Experimentally, it seems[1,2] that the columnar grains tend to form continuous rows in a direction perpendicular to the projection of the particle beam. This is easily understood in terms of the picture outlined above. Perpendicular to the beam, there is no long-range screening, and the lateral fluctuations are free to propagate. This leads to a more homogeneous structure in that direction. We expect then strongly anisotropic scaling properties, possibly with different scaling exponents perpendicular and parallel to the beam direction. This problem is currently under investigation.

Finally, we emphasize that an experimental verification of our results would be highly desirable. As a realization of the two-dimensional model, one could think of vapor deposition onto wires or fibers. The electrodeposition experiment of Matsushita, Hayakawa, and Sawada[49] has demonstrated, for the related case of diffusion-limited deposition,[31] the feasibility of extracting scaling exponents such as $\tau$ and $\nu_{\parallel}$ from experimental data. In fact, the screening mechanism responsible for the structures considered here is quite general and should be found in macroscopic systems also. One example is the aggregation of ice particles on electric wires and antennae in a steadily blowing snowstorm.[50]

*Note added in proof.* A numerical study of the cluster shape in on-lattice ballistic deposition onto a point seed was performed by Liang and Kadanoff.[53] They obtained a value of $32.0 \pm 0.5°$ for the growth angle $\psi$.

## ACKNOWLEDGMENTS

One of us (J.K.) wishes to thank Herbert Spohn for useful discussions, and Tim Halpin-Healy for sending him a copy of a paper prior to publication. He gratefully acknowledges support from the Deutsche Forschungsgemeinschaft.

## APPENDIX: GROWTH VELOCITY AND CLUSTER SHAPE

Here we relate the growth velocity as a function of the surface slope, $v(u)$, to the asymptotic shape of clusters grown by ballistic deposition onto a point seed.[14,23] A schematic picture of such a cluster is shown in Fig. 8(a). It consists of a lower triangular part with an opening angle $2\psi$ and a domed upper part. The dome joins the straight edges of the triangle at an angle $\alpha$ relative to the horizontal. The left and right corners of the cluster move apart at a rate $2v_{\perp}$, with $v_{\perp} = 1$ for the lattice model.

The domed surface constitutes the active zone of the cluster. Let $h(x,t)$ denote the height of the active zone above the $x$ axis, with $-v_{\perp}t \leq x \leq v_{\perp}t$. Asymptotically, the cluster attains an invariant growth shape,

$$h(x,t) = t\mu(x/t) \ , \tag{A1}$$

where the shape function $\mu$ is defined on the interval $[-v_{\perp}, v_{\perp}]$. A piece of the surface propagates at a speed determined by its slope $\partial h/\partial x$,

$$\frac{\partial}{\partial t} h(x,t) = v\left[\frac{\partial}{\partial x} h(x,t)\right] \ , \tag{A2}$$

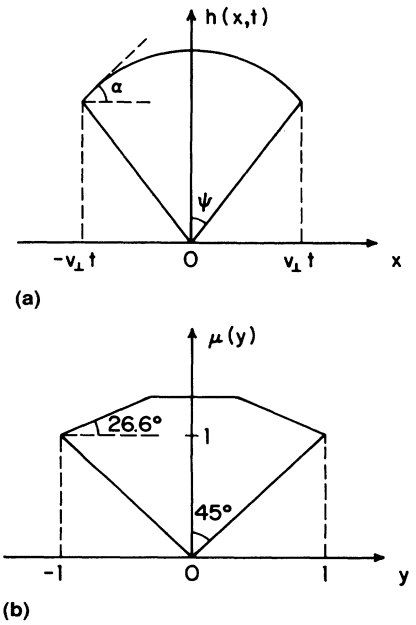


FIG. 8. (a) Schematic growth shape of a cluster grown by ballistic deposition onto a point seed at the origin. (b) Growth shape calculated from the growth velocity (3.31) of the $L = 2$ model.

where the function $v(u)$ is assumed to be given. Inserting (A1) into (A2), we get

$$\mu(y)-y\mu'(y)=v(\mu'(y)) \tag{A3}$$

which implies that $v(u)$ is the Legendre transform of $\mu(y)$. The two functions are thus related by

$$v(u)=\max_y [\mu(y)-uy] \tag{A4}$$

and

$$\mu(y)=\min_u [v(u)+yu] . \tag{A5}$$

This is equivalent to the well-known Wulff construction, which has been used to determine growth shapes of crystals[51] and Eden clusters.[52] Ramanlal and Sander[23] have presented a calculation of the growth shape of ballistic aggregates based on the tangent rule. Their result is recovered from (A5) with $v(u)=(1+u^2)^{1/4}$.

It is instructive to apply (A5) to the explicit expression (3.31) for the growth velocity of the $L=2$ model. In this case the cluster is grown from a point seed by simultaneous deposition at every other column of the infinite lattice, with a random choice of one of the two sets of columns at each time step. The reader is invited to carry out a few steps of this growth process. The resulting growth shape [Fig. 8(b)] is easily deduced from (3.31) by using the well-known fact that the Legendre transform takes vertices to edges and vice versa. The discontinuities in the slope of $v(\theta)$ at $\theta=0$ and $\theta=\theta_0=\arctan\frac{1}{2}$ give rise to facets of inclination $u=0$ and $u=\frac{1}{2}$. The facets join at $y=\frac{1}{3}$. The range $\theta\geq\theta_0$ maps onto the corners at $y=\pm 1$.

Conversely, the existence of sharp corners at $y=\pm v_\perp$ in the general case [Fig. 8(a)] forces $v(u)$ to be linear for large $u$. This is an immediate consequence of (A4). For large $u$, the maximum on the right-hand side is attained by choosing the smallest available value of $y$, $y=-v_\perp$, and hence

$$v(u)=\mu(-v_\perp)+v_\perp u . \tag{A6}$$

Since $\mu(-v_\perp)=v_\perp/\tan(\psi)$ [Fig. 8(a)] we have thus rederived Eq. (3.33). Moreover, it follows from (A4) that (A6) becomes exact when $\theta=\arctan(u)$ exceeds the corner angle $\alpha$.

For an estimate of $\alpha$, we return to the steady-state structure described in Sec. III C. The tip of a steady-state cluster [Fig. 4(b)] grows in the same manner as the corners of the cluster in Fig. 8(a). Thus asymptotically it has the shape of a sharp edge with opening angle $90°-\psi+\alpha$. From the plots shown in Fig. 4(b), we infer that $\alpha\simeq 60°-70°$. This is in qualitative agreement with the results of Sec. III C, where (A6) was found to hold for $\tan(\theta)\geq 2$.


[1]H. König and G. Helwig, Optik **6**, 111 (1950).
[2]H. J. Leamy, G. H. Gilmer, and A. G. Dirks, in *Current Topics in Materials Science,* edited by E. Kaldis (North-Holland, New York, 1980), Vol. 6; H. J. Leamy and A. G. Dirks, J. Appl. Phys. **49**, 3430 (1978).
[3]M. J. Vold, J. Colloid Sci. **14**, 168 (1959).
[4]D. Henderson, M. H. Brodsky, and P. Chaudhari, Appl. Phys. Lett. **25**, 641 (1977).
[5]A. G. Dirks and H. J. Leamy, Thin Solid Films **47**, 219 (1977).
[6]J. M. Nieuwenhuizen and H. B. Haanstra, Philips Tech. Rev. **27**, 87 (1966).
[7]N. G. Nakhodkin and A. I. Shaldervan, Thin Solid Films **10**, 109 (1972).
[8]T. Hashimoto, K. Okamoto, K. Hara, M. Kamiya, and H. Fujiwara, Thin Solid Films **91**, 145 (1982).
[9]O. Geszti, L. Gosztola, and E. Seyfried, Thin Solid Films **136**, L35 (1986).
[10]P. Meakin, P. Ramanlal, L. M. Sander, and R. C. Ball, Phys. Rev. A **34**, 5091 (1986).
[11]P. Meakin, Phys. Rev. A **38**, 994 (1988).
[12]T. A. Witten, Jr. and L. M. Sander, Phys. Rev. Lett. **47**, 1400 (1981).
[13]B. B. Mandelbrot, *The Fractal Geometry of Nature* (Freeman, New York, 1982).
[14]D. Bensimon, B. Shraiman, and S. Liang, Phys. Lett. **102A**, 238 (1984).
[15]P. Meakin, J. Colloid Interface Sci. **105**, 240 (1985).
[16]R. C. Ball and T. A. Witten, J. Stat. Phys. **36**, 873 (1984).
[17]F. Family and T. Vicsek, J. Phys. A **18**, L75 (1985).
[18]M. Kardar, G. Parisi, and Y. C. Zhang, Phys. Rev. Lett. **56**, 889 (1986).
[19]P. Meakin, J. Phys. A **20**, L1113 (1987).
[20]J. Krug, Phys. Rev. A **36**, 5465 (1987).
[21]J. Krug and H. Spohn, Phys. Rev. A **38**, 4271 (1988).
[22]J. Krug and H. Spohn, Europhys. Lett. **8**, 219 (1989).
[23]P. Ramanlal and L. M. Sander, Phys. Rev. Lett. **54**, 1828 (1985).
[24]S. Lichter and J. Chen, Phys. Rev. Lett. **56**, 1396 (1986).
[25]A. Mazor, D. J. Srolovitz, P. S. Hagan, and B. G. Bukiet, Phys. Rev. Lett. **60**, 424 (1988); D. J. Srolovitz, A. Mazor, and B. G. Bukiet, J. Vac. Sci. Technol. A **6**, 2371 (1988).
[26]M. Plischke and Z. Rácz, Phys. Rev. A **32**, 3825 (1985).
[27]R. Lipowsky and M. E. Fisher, Phys. Rev. Lett. **56**, 472 (1986).
[28]Z. Rácz and M. Plischke, Phys. Rev. A **31**, 985 (1985).
[29]R. Jullien and R. Botet, J. Phys. A **18**, 2279 (1985).
[30]H. van Beijeren, R. Kutner, and H. Spohn, Phys. Rev. Lett. **55**, 2026 (1985).
[31]Z. Rácz and T. Vicsek, Phys. Rev. Lett. **51**, 2382 (1983).
[32]M. Matsushita and P. Meakin, Phys. Rev. A **37**, 3645 (1988).
[33]S. Redner and A. Coniglio, J. Phys. A **15**, L273 (1982).
[34]D. Dhar, J. Phys. A **21**, L893 (1988).
[35]D. Forster, D. R. Nelson, and M. J. Stephen, Phys. Rev. A **16**, 732 (1977).
[36]D. E. Wolf and J. Kertész, Europhys. Lett. **4**, 651 (1987).
[37]D. Liu and M. Plischke, Phys. Rev. B **38**, 4781 (1988).

[38]R. Baiod, D. Kessler, P. Ramanlal, L. Sander, and R. Savit, Phys. Rev. A **38**, 3672 (1988).
[39]T. Halpin-Healy, Phys. Rev. Lett. **62**, 442 (1989); T. Nattermann (unpublished).
[40]M. Bramson and D. Griffeath, Ann. Prob. **8**, 183 (1980).
[41]M. Bramson and D. Griffeath, Z. Wahrscheinlichkeitstheorie verw. Gebiete **53**, 183 (1980).
[42]C. R. Doering and D. ben-Avraham, Phys. Rev. A **38**, 3035 (1988).
[43]J. L. Spouge, Phys. Rev. Lett. **60**, 871 (1988); J. Phys. A **21**, 4183 (1988).
[44]H. Kondoh, M. Matsushita, and Y. Fukuda, J. Phys. Soc. Jpn. **56**, 1913 (1987); H. Takayasu, I. Nishikawa, and H. Tasaki, Phys. Rev. A **37**, 3110 (1988).
[45]K. Kang and S. Redner, Phys. Rev. A **30**, 2833 (1984).
[46]P. Meakin and R. Jullien, J. Phys. (Paris) **48**, 1651 (1987).
[47]*Table of Integrals, Series and Products,* edited by I. S. Gradshteyn and I. M. Ryzhik (Adademic, New York, 1980).
[48]J. Kertész and D. E. Wolf, J. Phys. A **21**, 747 (1988).
[49]M. Matsushita, Y. Hayakawa, and Y. Sawada, Phys. Rev. A **32**, 3814 (1985).
[50]W. Kley (private communication).
[51]A. A. Chernov, Usp. Fiz. Nauk **73**, 277 (1961); Kristallografiya **7**, 895 (1962), *Modern Crystallography III: Crystal Growth,* Vol. 36 of *Springer Series in Solid State Sciences* (Springer-Verlag, Berlin, 1984).
[52]D. E. Wolf, J. Phys. A **20**, 1251 (1987).
[53]S. Liang and L. P. Kadanoff, Phys. Rev. A **31**, 2628 (1985).